On the Dissociation of N_2O after Electron Attachment†

H. U. Suter* and T. Greber

Physik Institut der Universität Zürich, Winterthurerstrasse 190, CH-8057 Zürich, Switzerland

Received: February 21, 2004; In Final Form: May 3, 2004

Total energy calculations were performed for nitrous oxide and its anion N_2O^- by Multi Configuration Self-Consistent Field−Configuration Interaction (MCSCF−CI) methods. The shape of the lowest unoccupied molecular orbital (LUMO) and the energy gap between the highest occupied molecular orbital (HOMO) are evaluated for different N_2−O distances and bending angles. The vertical electron affinities for the ground state and the first excited bending mode were found to be −2.1 eV, separated by about 50 meV. On the $^2A'$ potential energy surface (PES) of negatively charged N_2O the dynamics for the reaction after charge transfer on the ground state and thermally excited N_2O has been studied by wave packet calculations. The molecules dissociate within 30 fs and strong rotational excitation of the N_2 fragment is found. To explain the strong vibrational state selectivity we propose diabatic transitions between the $^2A'$ and the $^2A''$ PES to interrupt the dissociation of N_2O^- selectively. Implications for the dynamics of the Eley-Rideal reaction of N_2O on alkali metal surfaces are discussed in connection with exoemission experiments.

Introduction

In hot gas−surface reactions the intermediate products become hyperthermal and thus can walk on uncommon paths.[1] For the understanding of such reactions the exoemission experiments of Böttcher et al.,[2,3] where hot intermediate ions were inferred and the scanning tunneling experiments of Brune et al.,[4] where reaction fragments were found separated by large distances, brought new insight. The theoretical description of these nonequilibrium processes at surfaces is not simple, though there is some progress[5] beyond the picture of Nørskov et al.[6] Here we present a theoretical study that shall support interpretations of experiments on the dissociation of nitrous oxide after electron attachment. Experiments on the reaction of N_2O with alkali metal surfaces indicated three different reaction outcomes: N_2O may (i) scatter back into the gas phase, (ii) immediately dissociate upon impact (Eley-Rideal mechanism), or (iii) dissociate after adsorption (Langmuir−Hinshelwood mechanism).[7] More surprisingly this "trifurcation" is also observed if N_2O is fully defined, that is, state-selected *and* oriented at the beginning of the reaction.[8−10] The different reaction pathways were distinguished by measurements of the sticking probability and the detection of exoelectrons. Exoelectron emission indicates nonadiabatic reactions and probes the dynamics of charge-transfer processes in gas surface reactions.[11] In Eley-Rideal reactions it coincides with the impinging gas and reflects the deexcitation of a chemisorbing molecule where energies larger than the work function are released via Auger scattering of substrate electrons into a hole state on the reacting molecule and a free electron.

Figure 1 recalls the picture of Brandt et al.[10] for the Eley-Rideal reaction of N_2O with low work function surfaces. The reaction is triggered by *harpooning* of the impinging molecule.[12,13] Harpooning is the term adopted by Gadzuk for this type of reaction. It comprises resonant electron transfer on the *vertical* affinity level of the impinging molecule and its subsequent acceleration towards the surface. The vertical affinity level is the lowest unoccupied molecular orbital (LUMO) of the molecule. As outlined by Hellberg et al.[14] this vertical or Franck−Condon transition is the trigger of nonadiabaticity in gas surface reactions. Subsequently, the ionic species, here N_2O^-, is accelerated in the image field of the surface and starts to dissociate into $N_2 + O^-$. In the last step, where an exoelectron may be emitted, O^- reduces into O^{2-}.[8,15,16] From Figure 1b it becomes clear that resonance ionization (RI) occurs if the

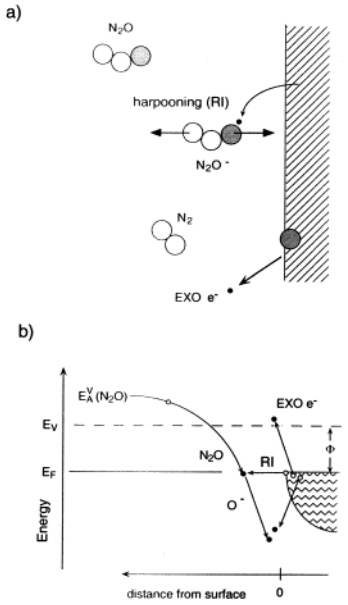

Figure 1. Eley-Rideal adsorption reaction of N_2O and its detection with exoelectrons. (a) The N_2O molecule approaches the surface. When the molecule is close to the surface it may be resonantly ionized (harpooned). Then the molecule accelerates and dissociates in the image field. The $O^- \rightarrow O^{2-}$ reaction may finally lead to Auger emission of an exoelectron (EXO e^-). (b) Same reaction in an energy diagram. At large distances from the surface the vertical affinity level E^V_A of N_2O lies above the vacuum level E_V. E^V_A lowers its energy in front of a surface with work function Φ. When it is degenerate with the Fermi level E_F, it may become resonantly ionized (RI). After dissociation the affinity level of the hot O^- species may dive nonadiabatically below the Fermi level and deexcite via the Auger emission of an exoelectron.

† Part of the special issue "Gerhard Ertl Festschrift".

10.1021/jp049204i CCC: $27.50
Published on Web 06/24/2004

LUMO, whose energy is lowered by the interaction with the surface, is degenerate with the Fermi level. To quantify the energy downshift of the LUMO, the work function and the *vertical* electron affinity in the vacuum have to be known. It is expected that this downshift mainly depends on the electron density at the surface and less on the kind of molecule. A measurement of the LUMO downshift is therefore a key quantity in order to decide whether a particular reaction may or may not proceed via harpooning.[13] The experiments of Brandt et al.[8−10] provide a handle for the determination of this affinity level downshift in a gas surface reaction. The exoemission in the Eley-Rideal channel from N_2O in the first excited bending mode ($\hbar\omega_2 = 73$ meV[17]) indicates for the case of N_2O/Cs(Li)/Pt(111) an energy downshift of the LUMO of 3.5 (4.4) eV.[8,10] In this context it is interesting to recall gas-phase experiments on dissociative attachment reactions ($N_2O + e^- \rightarrow N_2 + O^-$), where a strong reaction cross section dependence on the gas temperature, that is, on the bending mode occupancy, was found.[18,19]

It is the purpose of this paper to shed more light on the Eley-Rideal channel by quantum chemical calculations. It strongly depends on the history of the molecule in the gas phase and therefore gas-phase calculations are a good starting point. In particular, we investigated (i) the vertical electron affinity and its state dependence, (ii) investigated the geometrical shape of this affinity level, (iii) performed wave packet calculations on the adiabatic $^2A'$ potential energy surface of N_2O^- for the two N_2O^- states after electron attachment on $|JlM\rangle = |000\rangle$ ground state N_2O and $|111\rangle$ N_2O in its first vibrationally excited bending mode $n_2 = 1$,[20] and (iv) calculated the $^2A''$ potential energy surface that may affect the dissociation dynamics. We find the vertical affinity to depend on the bending angle and thus on the vibrational excitation of the molecule, though the difference is much smaller than expected from the classical vibration amplitudes and the potential model of Wren and Menzinger.[21] The rather isotropic shape of the LUMO cannot explain the dependence of the exoemission from the initial molecular orientation. And, for both ground state and vibrationally excited molecules, on the adiabatic PES direct dissociation occurs within 30 fs. The wave packet calculations demonstrate strong N_2 rotational excitation in the N_2O^- dissociation. The peculiar shape of the potential energy surface causes an unexpectedly small part of the available energy to couple into translational motion of O^-, which in turn influences the degree of nonadiabaticity and corresponding exoelectron yield. To understand the strong vibrational state dependence of the reaction outcome we discuss transitions from the adiabatic N_2O^- ($^2A'$) potential energy surface on the $^2A''$ surface. These two PES were related to whether the attached electron remains on the nitrogen molecule or on the oxygen atom after dissociation.

Methods of Calculation

A. Calculation of the Potential Energy Surface. The potential energy surfaces (PES) were calculated with the Molpro system of programs.[22] Internally contracted Multi Configuration Self-Consistent Field−Configuration Interaction (MCSCF−CI) calculations[23] were used for the evaluation of the energy. All calculations used C_s symmetry. The chosen atomic orbitals (AO) basis was the 6-31+G* set of Pople et al.[24] This resulted in 39 basis functions in a′ symmetry and 19 in a″ symmetry. The CI energy of the MCSCF−CI approach was finally modified with the Davidson correction. The active space consisted in 5 active orbitals (9a′, 10a′, 11a′, 2a″, and 3a″). The potential energy surface $V(R,\gamma,r_e)$ was calculated on a rectangular grid with 126 points in the Jacobi coordinates. The Jacobi coordinates for the NNO system are defined with R as the distance from the recoiling oxygen atom to the center of mass of N_2, and r_e is the intramolecular separation coordinate of the N_2 fragment. The angle γ is the angle between the N−N axis and the axis between O and the center of mass of N−N (see inset of Figure 3). This choice is justified by the simple form of the kinetic energy in the $N_2O^- \rightarrow N_2 + O^-$ reaction where $v_R = dR/dt$ is the velocity between N_2 and O^- and $\omega = d\gamma/dt$ the angular velocity of N_2. The kinetic energy E_{kin} then is

$$E_{kin} = \frac{1}{2}\mu v_R^2 + \frac{1}{2}\Theta\omega^2$$

where μ is the reduced mass of the oxygen atom and N_2 and Θ the moment of inertia of the N_2 fragment. The N−N bond distance $r_e = 1.13$ Å was kept constant.

B. Calculation of the Dynamics. Trajectories on the potential energy surface $V(R,\gamma,r_e = 1.13$ Å) were calculated by numerical integration of the Hamilton-Jacobi equations. The motion of N_2 and O after charge transfer was determined by time-dependent wave packet calculations. The potential was approximated on a grid of 128 points in each direction from the MCSCF−CI calculation mentioned above and a spline fit interpolation. The initial wave packet was placed at the coordinates of the N_2O initial state where for the propagation of the $|000\rangle$ ($|111\rangle$) state $R(t = 0) = 1.69$ Å (1.69 Å) and $\gamma(t = 0) = 180°$ (175.6°) were chosen. The width σ of the wave function $\psi(x) \propto \exp(-(x/\sigma)^2/2)$ is obtained from $\sigma_R^2 = \hbar/\mu\omega_1$ and $\sigma_\gamma^2 = \hbar/\Theta\omega_2$, where ω_1 and ω_2 are the frequencies of the corresponding vibrations, μ the reduced mass of N_2 and O, and Θ the moment of inertia of N_2. The vibrational energies from the B3LYP/6-31+G* basis set calculations are $\hbar\omega_1 = 167$ meV for the N−O stretch $\hbar\omega_2 = 75$ meV for the bending mode and $\hbar\omega_3 = 294$ meV for the N−N stretch. This results in $\sigma_R = 0.05$ Å and $\sigma_\gamma = 4.4°$.

As a propagator, the Feit−Fleck−Propagator $\hat{U}(t)$[25] was chosen

$$\hat{U}(\Delta t) = e^{-i(1/2)\hat{T}\Delta t}\, e^{-i\hat{V}\Delta t}\, e^{-i(1/2)\hat{T}\Delta t}$$

where $\hat{T}$ and $\hat{V}$ are the operators of the kinetic and potential energy, respectively. The integration step Δt is 0.1 fs. The program is an adapted version of the code used for the description of the photodissociation dynamics of FNO.[26] It uses a two-dimensional fast Fourier transform of a discrete wave function that is defined on a 64 times 64 grid. The portion of the wave packet that leaves the grid is deleted with the help of an optical potential.[27]

Results and Discussion

A. Geometry of N_2O and N_2O^-. The structure of N_2O and its anion are well-known and can be inspected in Figure 2a and b, respectively. In Tables 1 and 2 the optimized geometries of N_2O and N_2O^- are tabulated for various calculations. They compare well with the results of Hopper et al.[17] Notably, N_2O has a linear structure (NNO) and two double bonds of ≈1.1 Å. Upon electron attachment the adiabatically relaxed N−O bond distance is increased to 1.3 Å and the molecule bends to a N−N−O bond-angle Φ_{NNO} of 130° or $\gamma = 145°$. For the anion the optimized N−O bond length increases with the quality of the calculations, which indicates that the N−O bond is difficult to calculate.

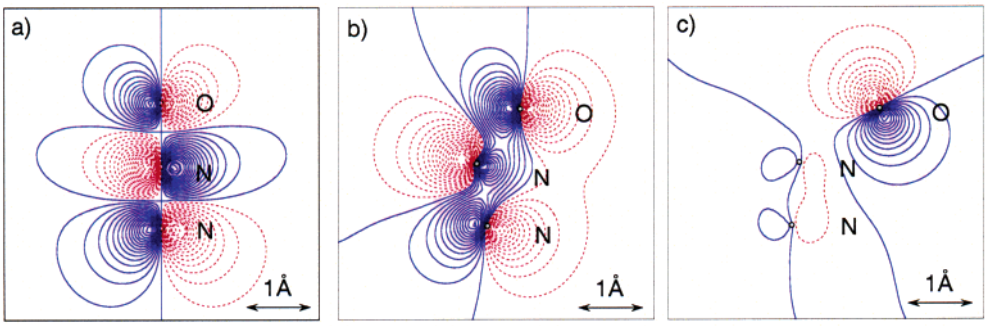

Figure 2. Contour plots of the molecular orbitals that are involved in the electron-induced N_2O dissociation. (a) The lowest unoccupied molecular orbital (LUMO) of N_2O (vertical affinity). (b) The highest occupied molecular orbital (HOMO) of N_2O^- at the coordinates with the lowest energy (adiabatic affinity). (c) The HOMO of $N_2 + O^-$ at coordinates where the charge is centered around the oxygen (dissociated state).

TABLE 1: Optimized Geometry of N_2O with Different Methods[a]

method	R_{N-N} (Å)	R_{N-O} (Å)	E (Ha)
HF/6-31+G*	1.085	1.171	−183.73209
MP2/6-31+G*	1.171	1.196	−184.21442
BLYP/6-31+G*	1.151	1.210	−184.66240
B3LYP/6-31+G*	1.132	1.195	−184.66830
QCISD/6-31+G*	1.136	1.209	−184.20058
MCSCF−CI/6-31+G*	1.146	1.207	−184.21014
MCSCF−CI/DZ[17]	1.147	1.240	−183.7819
QCISD(T)/avtz[31]	1.134	1.193	

[a] The bending angle $\Phi_{NNO} = 180°$ is kept constant.

TABLE 2: Optimized Geometry of N_2O^- as Obtained with Different Methods

method	R_{N-N} (Å)	R_{N-O} (Å)	Φ_{NNO} (deg)	E (Ha)
ROHF/6-31+G*	1.193	1.287	123.26	−183.66651
MP2/6-31+G*	1.185	1.324	130.34	−184.18667
BLYP/6-31+G*	1.214	1.335	133.75	−184.66441
B3LYP/6-31+G*	1.199	1.312	133.19	−184.67491
QCISD/6-31+G*	1.206	1.331	130.93	−184.19421
MCSCF−CI/6-31+G*	1.199	1.343	131.56	−184.19270
MCSCF−CI/DZ[17]	1.223	1.383	132.72	−183.7136
QCISD(T)/avtz[31]	1.196	1.320	133	

B. Frontier Orbitals. In the electron attachment reaction $N_2O + e^- \rightarrow N_2O^-$ the LUMO of N_2O is the most important frontier orbital. For linear N_2O it consists of degenerate antibonding π^* orbitals. With dissipation of excess energy this LUMO evolves into the HOMO of N_2O^-, or without dissipation upon dissociation into an O 2p orbital. In Figure 2 the wave functions of the LUMO of N_2O and the HOMOs of N_2O^- and O^- are shown in a contour plot. In Figure 2a the antibonding π^* character of the vertical affinity level (LUMO) is visible. It is interesting to note that the two ends of the molecule have similar weight. From this we conclude that the resonant charge transfer in the harpooning reaction should not depend strongly on whether the molecule approaches the surface by its N-end or by its O-end: It should occur at about the same center of mass distance of the molecule from the surface. In Figure 2b the adiabatic case, that is, the HOMO of N_2O^- in the equilibrium structure of N_2O^- is shown. In contrast to the LUMO of N_2O it has bonding character and the HOMO bond energy of adiabatic N_2O^- is strong enough to stabilize the N_2O^- ion (see below). In Figure 2c the nonadiabatic case is shown where N_2O^- dissociates into $N_2 + O^-$ and where the excess electron ends in the oxygen 2p shell. This O^- is the precursor state for the exoemission process where further charge transfer on the accelerated O^- ion leads to the emission of exoelectrons.[28]

C. Adiabatic Potential Energy Surface of N_2O^-. To describe the details of the dynamics of any reaction, the potential energy surface (PES) has to be known. First we limit ourselves to the two-dimensional adiabatic PES of N_2O^- where the bending angle γ and the N_2-O distance R span the phase space. The N=N bond length r_e is kept constant at 1.13 Å, the value of the neutral N_2O.

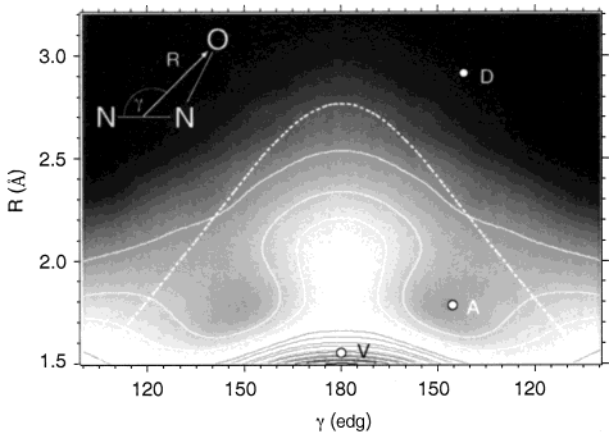

Figure 3. Contour plot of the $^2A'$ potential energy surface of N_2O^- as a function of the Jacobi coordinates R and γ. The used coordinates are shown in the inset. The energy difference between the contours is 0.271 eV. On the dashed line the Mullikan charge on the oxygen is 0.5 electron charges. The markers *V*, *A*, and *D* indicate the coordinates for the vertical, adiabatic, and dissociated molecular configurations as shown in Figure 2a, b, and c, respectively.

In Figure 3 the MCSCF−CI/6-31+G* method calculated potential energy surface (PES) of N_2O^- is shown together with the three points *V*, *A*, and *D*. These points indicate different geometries: the Franck−Condon or vertical transition geometry *V* with the N_2O coordinates, the "adiabatic" configuration *A* of the N_2O^- ground state, and *D*, where the PES is flat and where N_2O^- is dissociated into N_2 and O^-. The HOMO wave function at *V*, *A*, and *D* may also be inspected in Figure 2. The dashed line in Figure 3 corresponds to the geometrical configuration where the Mullikan charge on the oxygen is 0.5 electrons. Outside this line we consider the oxygen to be ionic.

The PES consists of a local maximum that we call the "Renner-Teller reef" along the linear configuration ($\gamma = 180°$) and a minimum A, near the equilibrium coordinates of N_2O^-. The Renner-Teller reef is very important for the dissociation starting from the Franck−Condon point. The Renner-Teller effect[29] drives the bending of the molecule where the additional electron lifts the degeneracy of π^* orbitals and a bonding and an antibonding orbital evolve with bending.[30]

The geometry *A* corresponds to a shallow minimum. A time-dependent calculation shows that the vibrational ground-state of the anion lives longer than pico seconds. The experimental determination of the lifetime of N_2O^- may be difficult since

TABLE 3: Adiabatic Electron Affinity $E^A_A = E(N_2O) - E(N_2O^-)$ of N_2O with the QCISD Geometries for N_2O and N_2O^- and Different Methods

method	$E(N_2O)$ (Ha)	$E(N_2O^-)$ (Ha)	E^A_A (eV)
HF/avtz	−184.74707	−183.67649	−1.92
MP2/avtz	−184.40507	−184.36368	−1.13
ACPF/avtz	−184.39599	−184.36776	−0.77
MR−CISD+DV/avtz	−184.40621	−184.38441	−0.59
MCSCF−CI/6-31+G*	−184.21014	−184.19270	−0.48
CCSD(T)/avtz	−184.42001	−184.40409	−0.43
QCISD/6-31+G*	−184.20058	−184.19421	−0.17
BLYP/avtz	−184.73174	−184.72868	−0.08
B3LYP/avtz	−184.73661	−184.73730	0.02
QCISD(T)/avtz[31]			−0.149
experiment[17]			0.22 ± 0.10

TABLE 4: Jacobi Coordinates and Energies of Selected Transition Points on the $N_2O(^1A')$ and $N_2O^-(^2A')$ Potential Energy Surfaces (r_e = 1.13 Å)[a]

transition point	R (Å)	γ (deg)	$E(N_2O)$ (Ha)	$E(N_2O^-)$ (Ha)	E_A (eV)	E_{avail} (eV)
$V_{\|000\rangle}$	1.69	180.0	−184.19949	−184.12258	−2.093	2.195
$V_{\|111\rangle}$	1.69	175.6	−184.19904	−184.12371	−2.050	2.164
reef	1.94	180.0	−184.18339	−184.12476	−1.595	2.136
A	1.78	145.0	−184.10384	−184.18145	2.112	0.593
D	2.95	140.0	−184.10736	−184.20325	2.609	0

[a] E_A is the energy difference $E(N_2O) - E(N_2O^-)$. E_{avail} is the available energy after electron attachment $E(N_2O^-)(X) - E(N_2O^-)(D)$. MCSCF−CI/6-31+G* method.

we expect the anion stability to depend on its vibrational state. However, the adiabatic equilibrium structure A is not expected to be reached upon electron attachment in the $N_2O + e^- \rightarrow N_2O^-$ reaction, because the excess energy between the vertical and the adiabatic electron affinity is much larger than the N_2O^- binding energy and may not be efficiently dissipated in a gas-phase reaction. Therefore, the long-discussed problem of the magnitude of the adiabatic electron affinity (E^A_A) is not of key importance for the dissociation dynamics. We nevertheless briefly discuss the state of the art of the theoretical determination of the adiabatic affinity. McCarthy et al.[31] concluded from a large QCISD calculation that the electron affinity of N_2O is negative, which would mean that the anionic system is metastable. This is contrary to experimental findings.[17] In Table 3 different results of the calculation of the electron affinity are presented. Only one of the calculations shows a positive E^A_A as does the experiment. Apparently, an accurate calculation of the electron affinity is difficult. One of the problems is the missing size consistency of some correlation schemes and the fact that differences between a potential energy surface of a charged and a neutral molecule are calculated without free parameters connecting the two. The calculations of McCarthy et al.[31] represent the state of the art and should have the correct size consistency. The results for E^A_A in Table 3 indicate that E^A_A is close to zero, though not even the sign is known. The conclusion is that the determination of E^A_A is not yet solved by ab initio theory and larger calculations are needed. It will, furthermore, be interesting to learn whether the recently proposed cyclic N_2O of Kryacho et al.[32] gives a further clue to the solution of the discrepancy between experiment and theory. Here the Kryacho anion complex is not considered since the experiments under investigation deal with stable and state prepared N_2O.

The vertical electron affinities $E^V_A(|000\rangle)$ and $E^V_A(|111\rangle)$ become −2.09 and −2.05 eV (see Table 4). These values constitute a decreasing energy on the N_2O^- PES and an increasing energy on the N_2O PES along γ. The present vertical electron affinities deviate from those that were estimated from the potential of Wren and Menzinger and the classical vibration amplitudes of the bending mode[33] (−2.2 and −1.5 eV).[8,13,21] In particular, the difference between the two decreases from 0.7 to 0.04 eV. We favor the present values that are based on a state of the art calculation. This has some implications for the interpretation of the experiments of Brandt et al.[8−10,13,34] It does not affect the statement that harpooning occurs in the reaction of N_2O with alkali metal surfaces that was proposed as well by Böttcher and Giessel.[15] The negative vertical electron affinities and the small energy difference between $E^V_A(|000\rangle)$ and $E^V_A(|111\rangle)$ translate, however, in very small differences in the harpooning distance of about 0.01 Å.[11] Therefore, the much smaller exoemission of N_2O in its vibrational ground state is not an indication for missing the condition of resonant charge transfer, it is rather a hint that there is no hot O^- species formed for the case of the $|000\rangle$ molecules. The main statements in the picture of Brandt et al. still hold and due to the increased value of $E^V_A(|111\rangle)$ the lower limits for affinity level downshifts increase to 4 and 4.9 eV for Cs and Li, respectively. From the similarities between the $|000\rangle$ and $|111\rangle$ states it must be conjectured that the reaction outcome is determined by the details of the dynamics after charge transfer.

D. Dynamics of the Dissociation. The dynamics of the N_2O^- dissociation were calculated for the two starting points $V_{|000\rangle}$ and $V_{|111\rangle}$ as given in Table 4. For the trajectories the initial kinetic energy was set to zero. For the wave packet calculations the wave function for the ground state is in harmonic approximation a Gaussian wave function with the parameters obtained for the vibrational parameters as described above. The $|111\rangle$ bending mode, centered at $V_{|111\rangle}$, corresponds to the first excited $n_2 = 1$ state.

In Figure 4 the trajectories and wave packet propagations for the N_2O $|000\rangle$ and the N_2O $|111\rangle$ states are shown after electron attachment on top of the N_2O^- PES for times t = 0, 12.5, and 25 fs. It can be seen that molecules in both states dissociate directly. For the $|000\rangle$ state the largest portion of the wave packet is strongly deviated by the Renner-Teller reef and indicates strong rotational excitation. Almost all of the wave packet is refracted out of the high-symmetry line ($\gamma = 180°$) and only a very small portion follows the linear dissociation channel across the Renner-Teller reef. The kinetic energy on the top of this reef is ≈ 40 meV. Such a bifurcation of a wave packet was found as well in the photodissociation dynamics of FNO in the first electronically excited state that strongly affects the partitioning of the available energy into the different degrees of freedom.[26] For the $|111\rangle$ state the wave packet follows nicely the trajectory and indicates as well a strong rotational excitation.

In Figure 5 the expectation values of the kinetic energy of the dissociating N_2O after electron attachment into the $|000\rangle$ and the $|111\rangle$ state is shown as a function of time. From Figure 5a it is seen that after 30 fs the available potential energy is transformed into kinetic energy. This time we take as the time for dissociation and the continuous kinetic energy increase indicates direct dissociation. Although the available energy differs for both starting points, $E^V_A(|000\rangle)$ and $E^V_A(|111\rangle)$, the dissociation time does not differ significantly. The offset of the kinetic energy at time $t = 0$ corresponds to the vibrational energies of the initial states. It has to be emphasized that this time for dissociation is a lower limit since it does not include any friction, nor does it include the fact that the attached electron may tunnel away from the oxygen and that the whole process does not necessarily everywhere obey the Born−Oppenheimer approximation. In the scenario of a gas surface reaction the electron (harpoon) does not reside all the time on the impinging

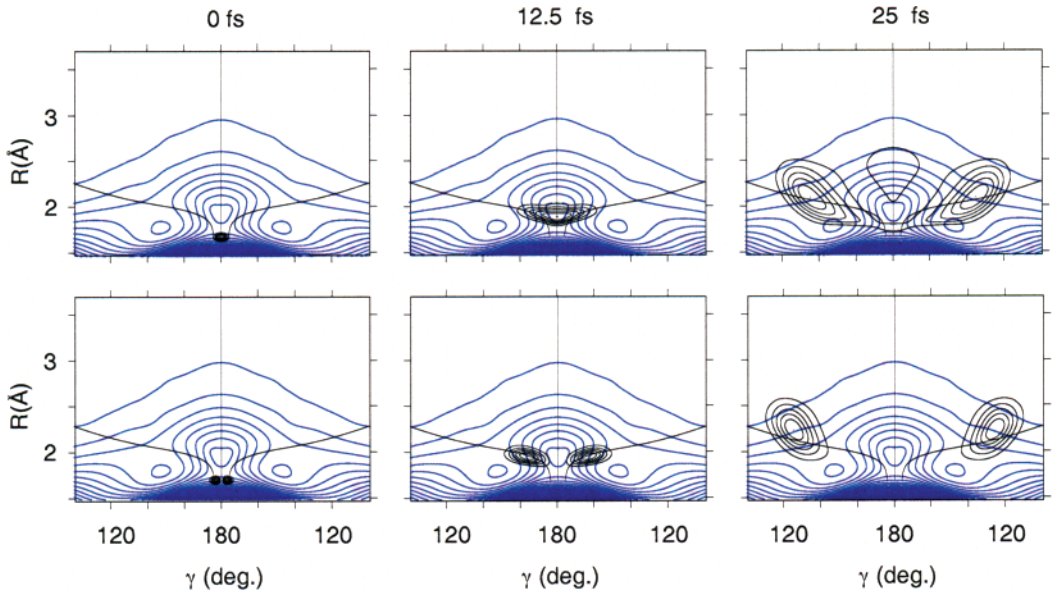

Figure 4. Snapshots of wave packet calculations on the N_2O^- potential energy surface as shown in Figure 3. The calculations were performed for $|000\rangle$ (top) and $|111\rangle$ (bottom) initial states and shown for 0, 12.5, and 25 fs after electron attachment to the N_2O molecules. The wave function square of the wave packets are superimposed as six contour-lines that were normalized to the maximum at any given time. Trajectories for E_{kin} ($R = 1.69$ Å, $\gamma = 180°$ and 175.6°) = 0 are indicated as well. It can be seen that on this potential energy surface both states dissociate directly.

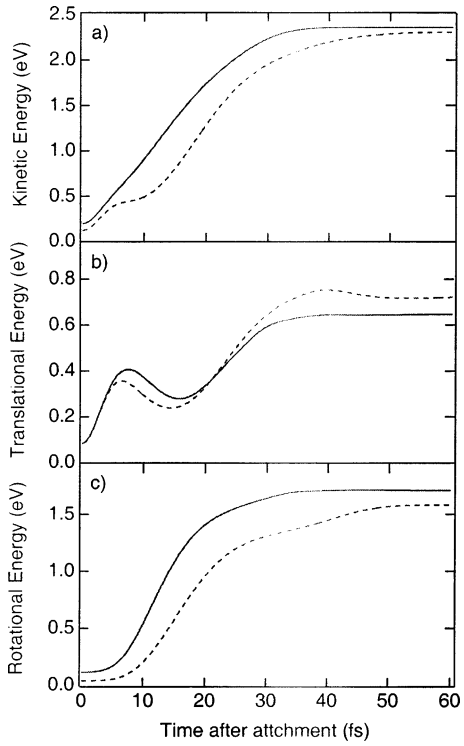

Figure 5. Kinetic energy and its partition versus time after electron attachment to $|000\rangle$ (dashed line) and $|111\rangle$ (solid line) N_2O. (a) Total kinetic energy, (b) translational kinetic energy, and (c) rotational kinetic energy. To obtain (b) the O translational energy in the rest frame, it has to be multiplied by 0.6.

molecule and the necessary action on the O^- that is needed for exoemission is reduced accordingly. In Figure 5b the expectation values of the translational energy are shown. This energy splits into a portion of the N_2 and a portion of the O^- fragment. The kinetic energy of the oxygen is the total translational kinetic energy multiplied by a factor of $\mu/m_O \approx 0.6$, where μ is the reduced mass of N_2 and O and m_O the oxygen mass. Clearly, the Renner-Teller reef decreases the translational energy after 6 and 8 fs. Though, 60 fs after electron attachment, the oxygen translational kinetic energy in the exit channels of $|000\rangle$ and $|111\rangle$ are almost identical (0.46 and 0.41 eV, respectively). In Figure 5c the expectation values of the rotational energy of the N_2 fragment is shown. For the $|000\rangle$ state the onset of rotation is delayed as is expected from the linear geometry. Though, after dissociation, the rotational energy exceeds that of the prebent $|111\rangle$ state. Furthermore, there is more energy transferred in the rotational than in the translational channel. This is a clear indication that the dissociation dynamics do not behave in a way as is expected from an impulsive model,[35] where all the available energy is partitioned at once into the different degrees of freedom along the breaking bond. In such a model for the N_2O^- dissociation there is no rotational excitation for the $|000\rangle$ state and the rotational excitation would always be smaller than the translational energy.

Although the linear bond breaking geometry favors vibrational excitation of the N_2 fragment, we expect it to be low. The small change of r_e in going from the N_2O equilibrium geometry to the N_2O^- equilibrium geometry, 7%, and the small corresponding energy gain upon relaxation of about 0.15 eV is less than one vibrational energy quantum of N_2 (0.29 eV). When this gas-phase dissociation scenario is implemented in a gas−surface reaction we expect the influence of the surface to be much stronger than the vibrational excitation of the N_2 fragment. In particular the Renner-Teller reef will change in front of a surface. On the background of the difficulties in calculating the adiabatic affinity in the gas phase accurately, it will remain important to perform experiments. It would therefore be interesting to measure the rotational state distribution of abstracted N_2.[9,36] The above findings on the dissociation do, however, emphasize that the strong state dependence of the exoelectron yield[8] may not be explained with different oxygen dynamics after electron attachment, nor a selective harpooning of $|111\rangle N_2O$.

A closer look to the potential energy landscape of the N_2O^- shows that besides the $N_2O^-(^2A')$ surface that leads to direct dissociation (see Figure 3) there is $N_2O(^1A')$ and an $N_2O^-(^2A'')$ surface. In the dissociation limit the $N_2O^-(^2A'')$ PES corresponds to $N_2^- + O$. The two potential energy surfaces for the anion originate from the degeneracy of the LUMO of linear N_2O. At

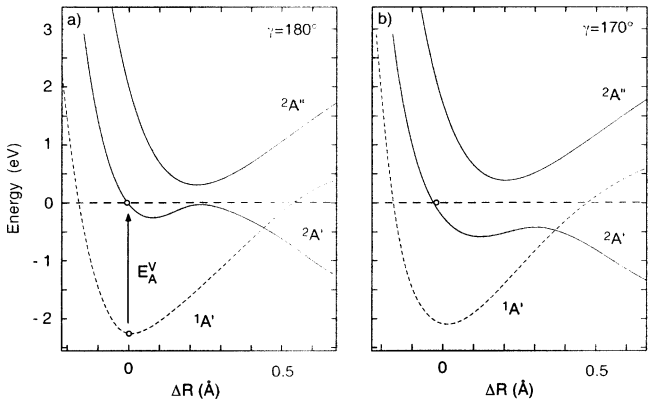

Figure 6. Potential energy curves along (a) $\gamma = 180°$ and (b) $\gamma = 170°$. The $N_2O^-(^2A')$ potential energy surface that leads to direct dissociation into $N_2 + O^-$, the $N_2O^-(^2A'')$, and the $N_2O(^1A')$ PES are shown. The vertical electron affinity E^V_A is indicated and points to the starting point of the dissociation process. The avoided crossing at the Renner-Teller reef, between $^2A'$ and $^2A''$, is proposed to significantly delay dissociation in the linear configuration ($\gamma = 180°$).

the Franck−Condon point on the $N_2O^-(^2A')$ PES the extra electron sits in the π orbitals which lie in the bending plane, while on the $N_2O^-(^2A'')$ PES the extra electron sits in the π orbitals that lie perpendicular to the bending plane. In Figure 6 the three involved surfaces are depicted on cuts along the *R*-coordinate. The lowest surface $N_2O(^1A')$, (dashed line) corresponds to the neutral molecule and is described as harmonic in γ and Morse-type in *R*. The relative energy position to the $^2A'$ surface is given by the vertical electron affinity E^V_A. The position of the reef is defined by the local maximum of $^2A'$ and the minimum of the $N_2O^-(^2A'')$ surface that is also bound similar to the neutral molecule. This further identifies the "reef" as a region of an avoided crossing; that is, a Landau−Zener region that is well-known as affecting the dynamics.[37] It is considered as the zone where the attached electron (harpoon) does not fulfill the Born−Oppenheimer approximation, and for larger distances *R* it remains on the oxygen ($^2A'$) or on the nitrogen ($^2A''$). The strong state dependence of the exoemission therefore emphasizes an inclusion of the $N_2O^-(^2A'')$ surface that may act as a dissociation inhibitor. From Figure 6 it can be seen that the energy difference $\Delta E_{12}(\gamma = 180°) \approx 0.3$ eV or coupling $\Delta_{12} = 1/2\ \Delta E_{12}$ between the two PES is strongest along $\gamma = 180°$ and is strongly angle dependent. Together with the Landau−Zener Formula,[34,38] which describes the tunneling or branching rate P_{branch} between the adiabatic ($^2A'$) and the diabatic ($^2A''$) PES of $P_{branch} = \exp(-2\pi\Delta_{12}{}^2/\hbar|\Delta F_{12}|v_\perp)$, where ΔF_{12} is the difference in force on the two PES without avoided crossing and $v_\perp$ is the velocity at the crossing, we see that the $^2A''$ state has a much stronger influence on the dynamics of the $|000\rangle$ state (Figure 6a) than on the $|111\rangle$ state (Figure 6b). It is likely that the anion in the $|000\rangle$ state has a higher probability to enter the $N_2O^-(^2A'')$ PES and that this may delay the dissociation. From the $^2A''$ PES the $N_2O(^1A')$ PES might be repopulated after electron back-donation.

IV. Summary, Conclusions, and Outlook

In summary the presented calculations indicate no strong dependence of the N_2O vertical electron affinity with the excitation of the vibrational bending mode. The geometrical shape of the vertical affinity level that is involved in the resonant charge transfer reaction at a surface is fairly isotropic, that is, not sensitive to N or O-end approaches to the surface. Therefore, harpooning should occur for all molecular orientations and vibrational excitations at the same distance, with the same probability. All observed differences in the reaction outcome must be related to the details of the dynamics after resonant ionization. Wave packet calculations where $|000\rangle$ and $|111\rangle$ states were propagated on an adiabatic N_2O^- potential energy surface indicate a high rotational excitation of the N_2 fragment that is even larger for the linear $|000\rangle$ state. The calculations emphasize that the released bond energy in N_2O^- substantially accelerates the O^- species that fuels the nonadiabaticity. Though, on the adiabatic PES no substantial difference in O^- terminal velocity is found for $|000\rangle$ and $|111\rangle$. The presented calculations confirm the model of Brandt et al. for the Eley-Rideal reaction of N_2O on Cs/Pt(100) and Li/Pt(100). They show affinity level downshifts in the order of 4 eV and subsequent gas−surface reactions in a hot ionic channel. We propose that the difference between $|000\rangle$ and $|111\rangle$ N_2O states involve a second potential energy surface and that the interaction with this surface delays the N_2O^- dissociation in such a way that much weaker exoemission occurs for ground state N_2O. In a next theoretical step the influence of the surface should be investigated beyond its role of an electron supplier.

Acknowledgment. Computer grants from the Swiss Center for Scientific Computing (SCSC) in Manno were essential for this study. We are grateful to the Schweizerischen Nationalfonds zur Förderung der wissenschaftlichen Forschung for financial support.

References and Notes

(1) Ertl, G. *Adv. Catal*. **2000**, *45*, 1.
(2) Böttcher, A.; Imbeck, R.; Morgante, A.; Ertl, G. *Phys. Rev. Lett.* **1990**, *65*, 2035.
(3) Greber, T.; Grobecker, R.; Morgante, A.; Böttcher, A.; Ertl, G. *Phys. Rev. Lett.* **1993**, *70*, 1331.
(4) Brune, H.; Wintterlin, J.; Behm, R. J.; Ertl, G. *Phys. Rev. Lett.* **1992**, *68*, 624.
(5) Kosloff, R.; Katz, G.; Zeiri, Y. *Faraday Discuss*. **2000**, *117*, 291.
(6) Nørskov, J. K.; Newns, D. M.; Lundqvist, B. I. *Surf. Sci.* **1979**, *80*, 179.
(7) Böttcher, A.; Niehaus, H. *Phys. Rev. B* **2001**, *64*, 045407.
(8) Brandt, M.; Greber, T.; Böwering, N.; Heinzmann, U. *Phys. Rev. Lett.* **1998**, *81*, 2376.
(9) Brandt, M.; Greber, T.; Kuhlmann, F.; Böwering, N.; Heinzmann, U. *Surf. Sci.* **1998**, *402-404*, 160.
(10) Brandt, M.; Kuhlmann, F.; Greber, T.; Böwering, N.; Heinzmann, U. *Surf. Sci.* **1999**, *439*, 49.
(11) Greber, T. *Surf. Sci. Rep*. **1997**, *28*, 3.
(12) Gadzuk, J. W. *Comm. At. Mol. Phys*. **1985**, *16*, 219.
(13) Greber, T. *Appl. Phys. A* **1998**, *67*, 701.
(14) Hellberg, L.; Strömquist, J.; Kasemo, B.; Lundqvist, B. I. *Phys. Rev. Lett.* **1995**, *74*, 4742.
(15) Böttcher, A.; Giessel, T. *Surf. Sci.* **1998**, *408*, 212.
(16) Hermann, K.; Freihube, K.; Greber, T.; Böttcher, A.; Grobecker, R.; Fick, D.; Ertl, G. *Surf. Sci*. **1994**, *313*, L806.
(17) Hopper, D. G.; Wahl, A. C.; Wu, R. L. C.; Tiernan, T. O. *J. Chem. Phys*. **1976**, *65*, 5474.
(18) Chantry, P. J. *J. Chem. Phys*. **1969**, *51*, 3369.
(19) Brüning, F.; Matejcik, S.; Illenberger, E.; Chu, Y. N.; Senn, G.; Muigg, D.; Denifl, G.; Märk, T. D. *Chem. Phys. Lett*. **1998**, *292*, 177.
(20) The nomenclature $|JlM\rangle$ is described in more detail in Parker, D. H.; Jalink, H.; Stolte, S. *J. Phys. Chem.* **1987**, *91*, 5427 and Choi, S. E.; Bernstein, R. B. *J. Chem. Phys.* **1986**, *85*, 150.
(21) Wren, D. J.; Menzinger, M. *Discuss. Faraday Soc.* **1979**, *67*, 97.
(22) Werner, H.-J.; Knowles, P. J.; Almlof, J.; Amos, R. D.; Berning, A.; Deegan, M. J. O.; Eckert, F.; Elbert, S. T.; Hampel, C.; Lindh, R.; Meyer, W.; Nicklass, A.; Peterson, K.; Pitzer, R.; Stone, A. J.; Taylor, P. R.; Mura, M. E.; Pulay, P.; Schütz, M.; Stoll, H.; Thorsteinsson, T.; Cooper, D. L. *MOLPRO*; package of ab initio programs.
(23) Werner, H. J.; Reinsch, E. A. *J. Chem. Phys.* **1982**, *76*, 3144.
(24) Francl, M. M.; Pietro, W. J.; Hehre, W. J.; Binkley, J. S.; Gordon, M. S.; Defrees, D. J.; Pople, J. A. *J. Chem. Phys.* **1982**, *77*, 3654.
(25) Feit, J. A.; Harris, J. R.; Feit, M. D. *J. Chem. Phys*. **1983**, *78*, 301.

(26) Suter, H. U.; Huber, J. R.; v. Dirke, M.; Untch, A.; Schinke, R. *J. Chem. Phys.* **1992**, *96*, 6727.
(27) Zhang, D. H.; Sharafeddin, O. A.; Zhang, J. Z. H. *Chem. Phys.* **1992**, *167*, 137.
(28) Greber, T. *Chem. Phys. Lett*. **1994**, *222*, 292.
(29) Renner, R. *Z. Phys.* **1934**, *92*, 172.
(30) Peyerimhoff, S. D.; Buenker, R. J. *J. Chem. Phys*. **1968**, *49*, 2473.
(31) McCarthy, M. C.; Allington, J. W. R.; Sullivan, K. O. *Mol. Phys*. **1999**, *65*, 1735.
(32) Kryachko, E. S.; Vincker, C.; Nguyen, M. T. *J. Chem. Phys.* **2001**, *114*, 7911.
(33) Jalink, H.; Harren, F.; van den Ende, D.; Stolte, S. *Chem. Phys.* **1986**, *108*, 391.
(34) Greber, T. *Curr. Opin. Solid State Mater. Sci.* **1998**, *3*, 446.
(35) Tuck, A. F. *J. Chem. Soc., Faraday Trans. 2* **1977**, *73*, 689.
(36) Böttcher, A. *Langmuir* **2000**, *16*, 8858.
(37) Domke, W.; Stock, G. *Adv. Chem. Phys.* **1997**, *100*, 1.
(38) Zener, C. *Proc. R. Soc. London, Ser. A* **1932**, *137*, 696.